University of Groningen

Excessive number of high asperities for sputtered rough films

Muravyeva, Tamara I.; Uvarov, Ilia V.; Naumov, Viktor V.; Palasantzas, George; Svetovoy, Vitaly B.

Published in:
Physical Review B

DOI:
10.1103/PhysRevB.104.035415

IMPORTANT NOTE: You are advised to consult the publisher's version (publisher's PDF) if you wish to cite from it. Please check the document version below.

Document Version
Publisher's PDF, also known as Version of record

Publication date:
2021

Link to publication in University of Groningen/UMCG research database

Citation for published version (APA):
Muravyeva, T. I., Uvarov, I. V., Naumov, V. V., Palasantzas, G., & Svetovoy, V. B. (2021). Excessive number of high asperities for sputtered rough films. *Physical Review B*, *104*(3), [035415]. https://doi.org/10.1103/PhysRevB.104.035415

Copyright
Other than for strictly personal use, it is not permitted to download or to forward/distribute the text or part of it without the consent of the author(s) and/or copyright holder(s), unless the work is under an open content license (like Creative Commons).

The publication may also be distributed here under the terms of Article 25fa of the Dutch Copyright Act, indicated by the “Taverne” license. More information can be found on the University of Groningen website: https://www.rug.nl/library/open-access/self-archiving-pure/taverne-amendment.

Take-down policy
If you believe that this document breaches copyright please contact us providing details, and we will remove access to the work immediately and investigate your claim.

Downloaded from the University of Groningen/UMCG research database (Pure): http://www.rug.nl/research/portal. For technical reasons the number of authors shown on this cover page is limited to 10 maximum.

Download date: 05-06-2022

Excessive number of high asperities for sputtered rough films

Tamara I. Muravyeva
Ishlinsky Institute for Problems in Mechanics, Russian Academy of Sciences, prospect Vernadskogo, 101-1, 119526 Moscow, Russia

Ilia V. Uvarov and Viktor V. Naumov
Valiev Institute of Physics and Technology, Yaroslavl Branch, Russian Academy of Sciences, Universitetskaya 21, 150007 Yaroslavl, Russia

George Palasantzas
Zernike Institute for Advanced Materials, University of Groningen - Nijenborgh 4, 9747 AG Groningen, The Netherlands

Vitaly B. Svetovoy*
A. N. Frumkin Institute of Physical Chemistry and Electrochemistry, Russian Academy of Sciences, Leninsky prospect 31 bld. 4, 119071 Moscow, Russia

(Received 27 April 2021; revised 20 June 2021; accepted 29 June 2021; published 12 July 2021)

The roughness of solids is crucial for interactions between bodies at short separations due to capillary or van der Waals–Casimir forces and for contact mechanics. Specifically, it is critical for the fabrication and operation of microelectromechanical systems, for which functional materials are deposited using thin film coating technologies. Here, it is demonstrated that the materials deposited by magnetron sputtering or thermally evaporated on a cold Si substrate reveal a significantly larger number of high asperities than that predicted by the normal distribution. Such asperities define the distance between the solids in contact that is the key parameter for many problems. The effect is related to the nonequilibrium deposition conditions and is suppressed if the material is deposited on a hot substrate or annealed. The high asperity tails can be described by the extreme value distribution or in some cases by the exponential distribution.

DOI: 10.1103/PhysRevB.104.035415

I. INTRODUCTION

The depositions of thin films of different materials by evaporation or magnetron sputtering [1,2] are widespread methods used in microtechnology for coating. An important characteristic of the deposited films is the surface roughness. The nanoscale roughness plays a crucial role in many areas of science and technology. The roughness is essential for heat transfer [3,4], contact resistivity [5,6], contact mechanics [7,8], and sealing and lubrication [9]. The nanoscopic roughness is important for capillary forces and wetting [10–12]. It is also very significant for experiments measuring the Casimir and van der Waals forces, when the distance between the interacting surfaces becomes comparable with the roughness amplitude [13–15].

The surface roughness is a factor that controls the occurrence of the pull-in instability. This instability is the main reason for the failure of microelectromechanical systems (MEMS) [16,17] when separate elements of MEMS stick permanently to each other due to irreversible adhesion. Since MEMS are fabricated using standard clean-room technology, the coating of the surfaces by sputtering or evaporation is relevant. The phenomenon of spontaneous stiction during fabrication or operation of MEMS has been investigated on a model system of an adhered cantilever [16,18] and the role of surface roughness has been confirmed by direct experiments [19]. The adhered cantilever, which does not suffer from a pull-in instability, has been proposed as a method to measure the Casimir forces at short separations inaccessible for the standard method of elastic suspension [15].

Atomic force microscopy (AFM) demonstrated that rough surfaces consist of peaks and pits [20–22] with a characteristic lateral size ξ (correlation length) and randomly distributed height with a root-mean-square (rms) value w. At lateral distances smaller than ξ the deposited metallic films show a self-affine character, when the height-height correlation function behaves as [23–25] $C_S(R) = w^2(R/\xi)^{2H}$, where H (<1) is the roughness exponent and R is the in-plane distance between two points. Typically, the height of peaks and pits is characterized by the normal distribution. In this case the elastic contact of a surface with the self-affine roughness and a flat surface can be described by Persson's theory [7]. However, this theory is applicable to very soft materials such as rubber, while for more stiff materials the situation can be different.

Real contact occurs on the highest asperities and for stiff materials the local pressure can be significantly larger than the nominal one. The local pressure can easily exceed the flow stress resulting in plastic deformations [15] so that the contact is no longer elastic. Moreover, the height distribution of the asperities can differ from the normal distribution especially for high asperities. It was demonstrated for gold films thermally evaporated on silicon wafers [26]. The peaks with a height of $(2-3)w$ follow the normal distribution but higher asperities appear more often than predicted by the normal distribution.

*Corresponding author: svetovoy@yandex.ru

 ©2021 American Physical Society

Because real contact is realized on these high peaks, they play a significant role in the contact problem.

High peaks are rare statistical events and the lateral distance between them is large in comparison with the correlation length. For this reason the smaller the size of the investigated area, the smaller is the height of the highest peak in this area. The dependence on the area size has been demonstrated for gold films of different roughnesses [26]. When one investigates a small area as, for example, for colloid particles [27], a normal distribution for the asperities is justified, but already for nominal interaction areas of $1 \times 1\ \mu m^2$ or larger the normal distribution fails to describe the situation [14,26]. Thus, high asperities are very important for the problem of contact and for interactions between solids at distances comparable with the height of these asperities. However, at this moment, an excessive number of high peaks was observed only for oligomer [28] and Au [26] thin films thermally deposited on Si substrates and it is not clear how general is this phenomenon.

In this paper, based on the analysis of large area AFM scans supported by the images from a scanning electron microscope (SEM), we demonstrate that significant deviations from the normal distribution is not an exceptional property. All the tested films of Cu, Pt, W, and SiO_2 deposited by magnetron sputtering on a Si substrate at room temperature show a significant number of high peaks, which can be described by an extreme value distribution. The finding is important for the description of the interaction between solids close to or being in contact.

II. MATERIALS AND METHODS

Films of W, Pt, Cu, and SiO_2 were deposited using magnetron sputtering by SCR-651 Tetra (Alcatel). Pressure in the vacuum chamber was reduced to $5 \times 10^{-4}\ \mu$bar with a turbomolecular pump. Argon was used as a working gas at a pressure 2 μbar for deposition of all the metals and 13% of O_2 was added to Ar for the deposition of SiO_2 (total pressure 2.2 μbar). The sputtering system operates at 13.56 MHz; the power at the target was 300 W for the deposition of tungsten and 200 W for the other materials. A thin (10-nm) adhesive sublayer of Ti was used to deposit the metals. The deposition rates were (in nm/s) 0.42 (W), 0.28 (Pt), 1.00 (Cu), and 0.17 (SiO_2). The films were deposited at room temperature, but Pt and W films were deposited also on hot substrates at 400 and 600 °C, respectively. Two tungsten films deposited at room temperature were annealed without breaking the vacuum at 600 °C during 30 min. The film thicknesses were 100 and 300 nm for W, 100 and 200 nm for Pt, 100, 250, 500, and 750 nm for Cu, and 312, 420, 878, and 990 nm for SiO_2.

The roughness of the films was investigated with a SmartSPM 1000 (AIST-NT) AFM instrument in the tapping mode. The cantilevers fpN10 (AIST-NT) had a nominal spring constant 11.5 N/m, resonance frequency 250 kHz, and tip curvature radius 10 nm. The data were collected from $1 \times 1\ cm^2$ samples in three arbitrarily chosen locations for each sample. For the determination of the roughness distribution the scan area was $20 \times 20\ \mu m^2$ with a resolution of 4096 pixels per line. It was possible to collect high resolution data from this large area due to the high stability of the recording system and a low level of vibrations. Smaller images $5 \times 5\ \mu m^2$ with 1024 pixels per line were collected only for SiO_2 films. The correlation lengths of the films were determined from $2 \times 2\ \mu m^2$ scans with 1024 pixels per line. For comparison we provide also the data for a 200-nm-thick Au film thermally evaporated as described in Ref. [26]. For the gold sample the data were collected with a Bruker Multimode 8 AFM. For all samples the topographical features visualized with AFM were controlled with the scanning electron microscope (SEM) Zeiss Supra 40. The parameters characterizing the sputtered films are collected in Table S1 [29].

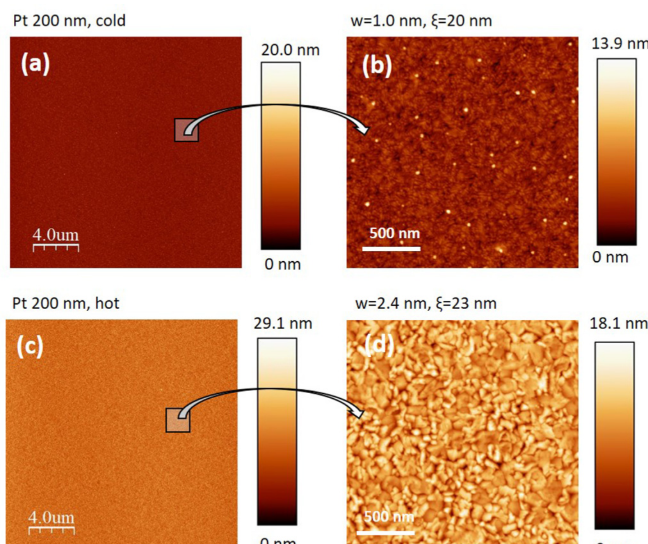

FIG. 1. (a) AFM image of Pt film with an area of $20 \times 20\ \mu m^2$ deposited on a Si substrate at room temperature (cold). The color bar shows the height scale. (b) A zoomed $2 \times 2\ \mu m^2$ area taken from the full image. (c) The same as (a) but the film is deposited on a hot substrate at $T = 400\,^{\circ}$C. (d) Magnified view of the film in (c).

III. RESULTS

Since we are looking for high asperities, which are statistically rare events, it is important to collect information on the roughness from as large an area as possible. On the other hand, the spatial resolution has to be sufficient to resolve separate asperities. These are contradictory conditions so that a scan area of $20 \times 20\ \mu m^2$ and a number of pixels per line of 4096 were chosen to keep the balance between the two conditions within the range of the AFM instrument. These parameters correspond to a pixel size of 4.88 nm. From such a megascan one can get information on different length scales. This approach proposed in Ref. [26] also guarantees that the information corresponds to a homogeneous area on the sample in contrast with smaller separate scans.

Figure 1(a) shows a full scan of the Pt film deposited on a Si substrate at room temperature. Since the resolution is high, one can see in Fig. 1(b) the magnified details from an area 10 times smaller in size than the original scan. The grain structure can be seen in this image, but unexpectedly high peaks comparable in lateral size with the grains are also visible. These peaks cannot be treated as dust because their aspect ratio (width/height) is about 5 and their number is large. Moreover, the film deposited on the Si substrate at $T = 400\,^{\circ}$C shown in Figs. 1(c) and 1(d) does not demonstrate

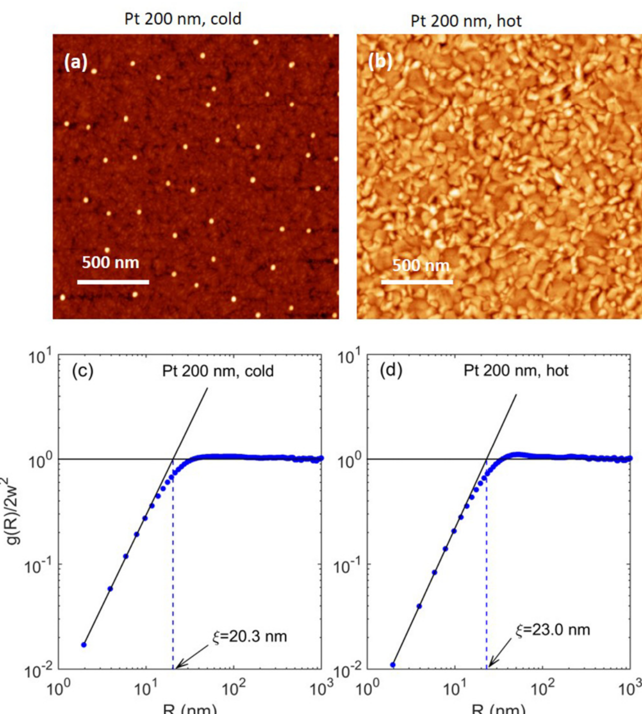

FIG. 2. (a) and (b) AFM image of Pt films with an area of $2 \times 2\ \mu\text{m}^2$ and a pixel size of 1.95 nm deposited on a cold and hot substrate, respectively. (c) and (d) The height-difference correlation function (circles) extracted from the images in (a) and (b). The solid black lines show the asymptotics corresponding to Eq. (2). The blue dashed line indicates the correlation length.

similar peaks although it was processed in the same way as the film deposited on a cold substrate.

To determine the correlation length ξ one has to use a better spatial resolution. For this purpose we used AFM scans with an area $2 \times 2\ \mu\text{m}^2$ and 1024 pixels per line (the pixel size is 1.95 nm). The height-difference correlation function is defined as

$$g(R) = \frac{1}{A}\int dxdy[z(\mathbf{r}+\mathbf{R}) - z(\mathbf{R})]^2, \tag{1}$$

where $z(\mathbf{r})$ is the height in the point $\mathbf{r} = (x, y)$, $\mathbf{R} = \mathbf{r}' - \mathbf{r}$ is the distance between the points, and A is the area of the image. All the investigated materials demonstrate a self-affine roughness that is characterized by the following asymptotic behavior [25,30,31],

$$\frac{g(R)}{2w^2} = \begin{cases} (R/\xi)^{2H}, & R \ll \xi, \\ 1, & R \gg \xi. \end{cases} \tag{2}$$

Figures 2(a) and 2(b) show these higher resolution images of 200-nm-thick Pt films deposited on cold and hot substrates, respectively. Comparing these images with those in Figs. 1(b) and 1(d) produced from the megascans one can see the increase in the resolution does not change the images. The high resolution images are important only for the determination of the correlation length. The functions $g(R)$ are shown in Figs. 2(c) and 2(d), from which ξ can be determined. In this way the correlation length has been determined for all the materials.

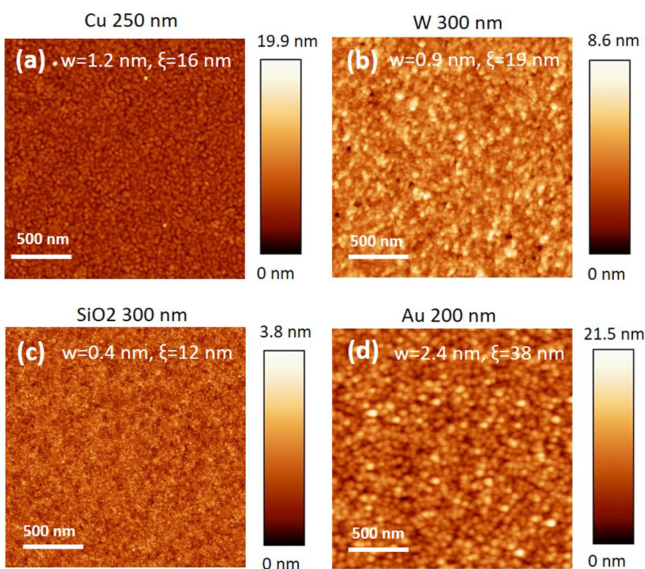

FIG. 3. (a)–(d) $2 \times 2\ \mu\text{m}^2$ areas of the full images for Cu, W, SiO_2, and Au, respectively, deposited at room temperature.

The observed difference in the topography of the films deposited on cold and hot substrates is supported by SEM images (see Fig. S1). To see also the similarity between SEM and AFM images one has to take into account that SEM keeps the horizontal and vertical scales approximately the same, while for AFM the lateral scale is typically much larger. For this reason high peaks in Fig. 1(b), which are roughly 30 nm wide and 10 nm high, appear as bright spots in AFM but are barely visible in the SEM images. Nevertheless, adjusting the contrast of SEM images one can see the similarity with the AFM images as Fig. S1(e) shows.

Magnified views of the Cu, W, SiO_2, and Au films deposited on cold Si substrates are shown in Fig. 3. These films demonstrate very different roughnesses but all of them contain a significant number of asperities with heights much larger than the rms roughness. These high peaks are not so well pronounced as for Pt, but they are clearly visible in histograms (see Fig. 4 below). On the other hand, similar to Pt, tungsten deposited on a hot substrate or annealed at 600 °C after the deposition, does not show an excessive number of high peaks as one can see in Fig. S4. We assume that the high asperities are related to the nonequilibrium deposition conditions. These conditions result in a smaller rms roughness with more significant deviations from the average height of the asperities. If the film is deposited on a hot substrate, it is closer to the equilibrium due to faster surface diffusion. Similarly, the surface diffusion is involved when the film is annealed.

The height probability density function is constructed from the AFM images as a histogram. It is defined as a number of pixels with heights within the interval $(z, z + \Delta z)$ normalized to the total number of pixels and to the size of the bin Δz, where z varies from 0 to $z_{\max}$ (the highest pixel in the image). The data collected in this way are presented in Fig. 4, where the height $x = z - z_{\text{av}}$ is counted from the average value z_{av}, so that the average position of the surface corresponds to $x_{\text{av}} = 0$.

If the scans are taken from different places in the sample, the distribution function is well reproducible, as one can see

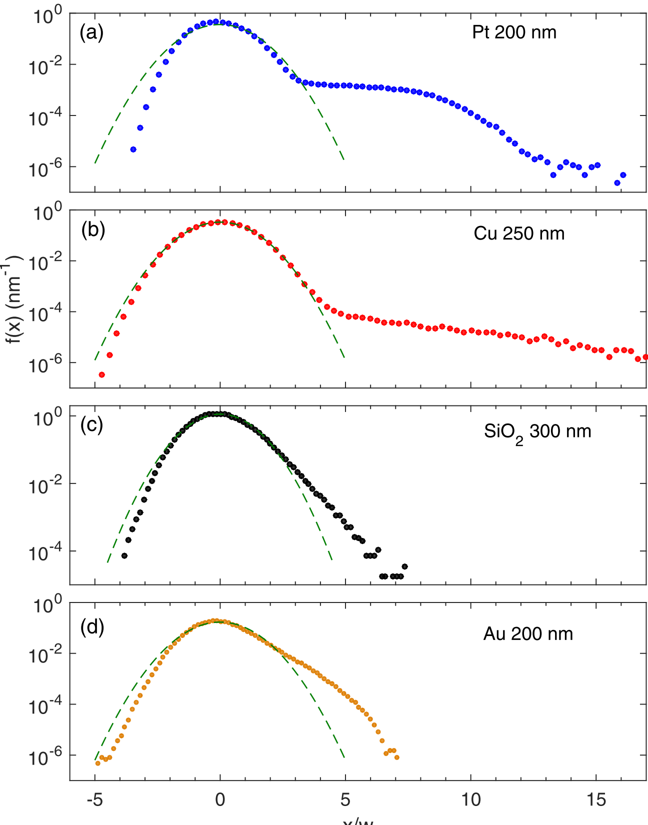

FIG. 4. Probability density function for different materials deposited on a Si substrate at room temperature. The green dashed curve shows the normal distribution for the same rms roughness.

in Fig. S2 for Pt and Cu. For very high peaks (large x/w) some scattering of the data is due to the small number of peaks. We have to note that for small area scans the scattering is significant, which makes it difficult to collect a reliable statistics of high peaks. It is one of the reasons to use megascans for the data collection. Figure S3 illustrates that by using a linear vertical scale for the distribution function it is not possible to see a strong deviation from the normal distribution.

The density function can be compared with the normal (Gaussian) distribution function,

$$f_n(x) = \frac{1}{w\sqrt{2\pi}} \exp(-x^2/2w^2). \quad (3)$$

The function $f_n(x)$ depends only on one parameter w. Choosing this parameter to be equal to the rms roughness of the film determined from the scan, we get the corresponding normal distribution for the film. For each graph in Fig. 4 this distribution is shown by the green dashed curves. One can see that all the materials deposited at room temperature demonstrate a significant deviation from the normal distribution for high asperities. We call the part of the observed distribution which deviates from the normal one the high peak tail. Although the probability to find a high peak is low, there are many such peaks on a large area. These rare peaks will define the actual contact between solids. The high peak tail (peaks with $x \gtrsim 3w$) is especially well pronounced of Pt and Cu, while for SiO_2 and Au the tail is not so long. Tungsten, which is not

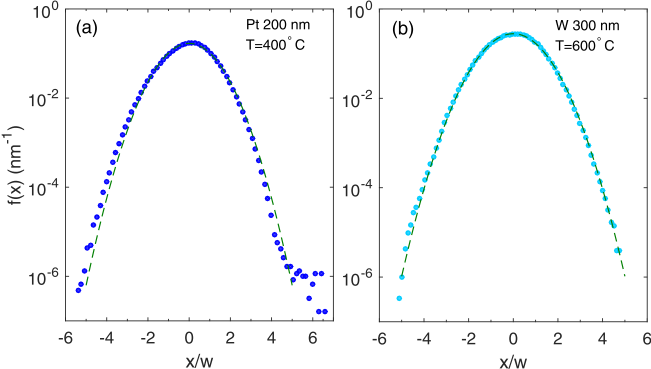

FIG. 5. Probability density function for Pt and W deposited on hot Si substrates. The normal distribution (green dashed curve) describes well the observed distribution.

shown in Fig. 4, can have a tail comparable with that for Pt and Cu or with that for gold as one can see in Figs. S4(a) and S4(c).

To feel the difference between the actual and normal distributions let us provide a few numbers. At $x = 5w$ for Pt, $f_n(5w) = 1.34 \times 10^{-6}$, but the actual value is $f(5w) = 1.47 \times 10^{-3}$. The probability to find a peak with a height of $5w$ is three orders of magnitude larger than that for the normal distribution. For other materials the ratio $f(5w)/f_n(5w) \sim 100$ is somewhat smaller but still very large.

Figure 5 shows the probability density function extracted from the images of platinum and tungsten films deposited on a hot substrate. The difference with Fig. 4 is striking. The materials deposited on a hot substrate have practically no excessive high peaks in comparison with the normal distribution. A similar situation is observed for annealed tungsten films [see Fig. S4(d)].

The existence of the high peak tail was already noted for the thermally evaporated gold films [26]. It was suggested [32] that for Au films the tail can be described by the extreme value distribution [33], for which the cumulative distribution can be presented in the form

$$P(x) = 1 - \exp[-e^{(x-\mu)/\beta}], \quad x \gtrsim 3w, \quad (4)$$

where μ and β are the parameters. However, it was not clear how general is such a behavior. This paper demonstrates that a significant deviation from the normal distribution is a generic feature for all the investigated materials magnetron sputtered on a cold substrate. The degree of deviations and the details of the high peak tail can be specific for each material. Nevertheless, one can make some statements about the distribution of high asperities.

The total number of pixels in a megascan is $N = 2^{2\times12} \approx 1.68 \times 10^7$. The number of pixels with the height h larger than x is $N_h(x) = N[1 - P(x)]$. This number as a function of x is shown in Fig. 6 for different materials. The gold film in Fig. 6(a) is well described by the extreme value distribution (4) in the interval $2.5w < x < 7w$, in agreement with Refs. [14,32] where rougher films have been analyzed. The first point of the interval is the place where the actual distribution starts to deviate from the normal one. The numbers

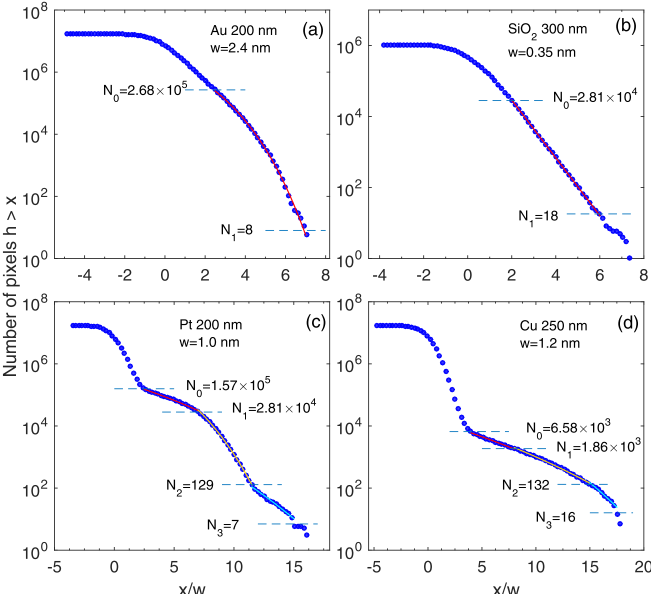

FIG. 6. Number of pixels with a height h larger than a given value x for different materials. The data for high peaks are fitted with (4) or with the exponential distribution (for SiO_2). For Pt and Cu the data are fitted piecewise by the extreme value distribution. The numbers at the breakpoints show the number of pixels for the corresponding x.

near the horizontal dashed lines are the number of pixels at the beginning and the end of the interval. A very smooth SiO_2 film with fine lateral features [Fig. 6(b)] is described better by the exponential distribution $1 - P(x) \sim \exp(-x/w)$ in the interval $2w < x < 6w$ than by the extreme value distribution. The high pixels outside of the interval are related to one or a maximum of a few highest peaks and have no statistical significance.

The films of Pt and Cu have a more complicated structure of the cumulative distribution. Nevertheless, the high peaks for these materials can be described by the extreme value distribution in a piecewise way. In this case one can separate three domains described by the extreme value distribution but with different parameters. For platinum these domains are located between the breakpoints $x = 2.5w, 7w, 11.5w, 15w$. As one can see in Fig. 6(c), the fitting with the piecewise parameters describes the cumulative distribution for Pt nearly perfectly. In a similar way one can describe the distribution for Cu [Fig. 6(d)], but the breakpoints are different: $x = 4w, 8w, 15w, 17.5w$. In comparison with Pt, the normal distribution can be applied to Cu up to $x = 4w$ but qualitatively the high peak tails behave similarly. This similarity suggests that the physical processes responsible for different domains also have to be similar. The piecewise behavior means that there are three groups of high peaks, which are described by different parameters μ and β in (4).

Of course, the film deposition in plasma is a complicated process and we can only speculate on the physical origin of the high peaks. We relate the occurrence of high peaks with the relaxation of local stresses, which appear during the nonequilibrium film growth. For metals this process is described by the extreme value statistic, but for SiO_2 the statistics can be different because, in contrast with plastic metals, silicon oxide is a brittle material. A very long tail of the distribution for Pt and Cu can be explained by the existence of different kinds of stress centers, which are described by different parameters of the extreme value distribution. These high peaks are, however, metastable and can disappear at high temperatures.

The numbers shown in Fig. 6 near the breakpoints indicate the number of pixels with the height larger than the break value of x. These numbers, however, do not correspond to the number of high peaks. It is possible to establish the correspondence between the number of pixels and the number of peaks assuming a specific shape of the peaks. However, as a rough estimate we assume here that the area of one peak is $\pi r^2/2$, where r is related to the correlation length as $r = \xi/2$. For $\xi = 20$ nm and the area of one pixel 23.8 nm^2, one finds about 7 pixels per peak. Thus, from Fig. 6 one can conclude that the last breakpoint corresponds to one or a few peaks, but a significant number of peaks exist for smaller values of x.

From the theoretical point of view it was suggested [28] that the non-Gaussian height distribution is explained by the roughening mechanism described by the Kardar-Parisi-Zhang (KPZ) scenario [34]. This idea has been analyzed in Ref. [35] where the role of the extreme value distribution has been stressed. The current paper shows that the KPZ model of film growth is plausible, but more theoretical work is needed to explain the exponential distribution for SiO_2 films and breaking points for Cu and Pt.

IV. CONCLUSIONS

We collected detailed information on roughness of thin films magnetron sputtered on a substrate using large area AFM megascans containing $\sim 10^7$ pixels. We observed that the deposition of different materials on a cold substrate (magnetron sputtered or thermally evaporated) provides the films with a significant number of high asperities that exceed considerably the number predicted by the normal distribution of roughness. On the other hand, if the films are deposited on a hot substrate or annealed, they are well described by the Gaussian distribution. We concluded that the finding is related to the nonequilibrium deposition conditions. For all metallic films the high peaks can be well described by the extreme value statistics. Platinum and copper, which demonstrate long tails in the distribution of high peaks, are also described by the same statistics but in a piecewise way. In contrast the SiO_2 film is described much better by the exponential distribution. These observations are very important for interactions between solids at short separations and for contact mechanics, when the thin film coating technology is used as, for example, in MEMS. The excessive number of high peaks is crucial for the explanation of the Casimir forces measured at distances comparable with the height of these peaks or even when the surfaces are in direct contact.

ACKNOWLEDGMENTS

We are grateful to Mikhail Savvateev for technical assistance with large size AFM scans. T.I.M., I.V.U., and V.B.S. acknowledge support from the Russian Science Foundation,

Grant No. 20-19-00214, G.P. acknowledges support from the Netherlands Organization for Scientific Research (NWO) Grant No. 16PR3236. The original AFM scans and SEM images are available upon the request from V.B.S.

---

[1] A. Barranco, A. Borras, A. R. Gonzalez-Elipe, and A. Palmero, Perspectives on oblique angle deposition of thin films: From fundamentals to devices, Prog. Mater. Sci. **76**, 59 (2016).

[2] H. Angus Macleod, Recent developments in deposition techniques for optical thin films and coatings, in *Optical Thin Films and Coatings*, edited by A. Piegari and F. Flory, Woodhead Publishing Series in Electronic and Optical Materials (Woodhead Publishing, Sawston, Cambridge, UK, 2013), pp. 3–25.

[3] J.-F. Zhao, A.-L. Wang, and C.-X. Yang, Prediction of thermal contact conductance based on the statistics of the roughness profile characteristics, Int. J. Heat Mass Transfer **48**, 974 (2005).

[4] A. I. Volokitin and B. N. J. Persson, Near-field radiative heat transfer and noncontact friction, Rev. Mod. Phys. **79**, 1291 (2007).

[5] E. Rabinowicz, *Friction and Wear of Materials* (Wiley, New York, 1995).

[6] F. M. Mwema, O. P. Oladijo, S. A. Akinlabi, and E. T. Akinlabi, Properties of physically deposited thin aluminium film coatings: A review, J. Alloys Compd. **747**, 306 (2018).

[7] B. N. J. Persson, Relation between Interfacial Separation and Load: A General Theory of Contact Mechanics, Phys. Rev. Lett. **99**, 125502 (2007).

[8] M. H. Müser, W. B. Dapp, R. Bugnicourt, P. Sainsot, N. Lesaffre, T. A. Lubrecht, B. N. J. Persson, K. Harris, A. Bennett, K. Schulze *et al.*, Meeting the contact-mechanics challenge, Tribol. Lett. **65**, 118 (2017).

[9] B. N. J. Persson, *Sliding Friction: Physical Principles and Applications* (Springer, Heidelberg, 2000).

[10] F. W. DelRio, M. L. Dunn, L. M. Phinney, C. J. Bourdon, and M. P. de Boer, Rough surface adhesion in the presence of capillary condensation, Appl. Phys. Lett. **90**, 163104 (2007).

[11] P. J. van Zwol, G. Palasantzas, and J. T. M. De Hosson, Influence of roughness on capillary forces between hydrophilic surfaces, Phys. Rev. E **78**, 031606 (2008).

[12] G. H. ten Brink, N. Foley, D. Zwaan, B. J. Kooi, and G. Palasantzas, Roughness controlled superhydrophobicity on single nanometer length scale with metal nanoparticles, RSC Adv. **5**, 28696 (2015).

[13] P. J. van Zwol, G. Palasantzas, and J. T. M. De Hosson, Influence of random roughness on the Casimir force at small separations, Phys. Rev. B **77**, 075412 (2008).

[14] W. Broer, G. Palasantzas, J. Knoester, and V. B. Svetovoy, Roughness correction to the Casimir force at short separations: Contact distance and extreme value statistics, Phys. Rev. B **85**, 155410 (2012).

[15] V. B. Svetovoy, A. V. Postnikov, I. V. Uvarov, F. I. Stepanov, and G. Palasantzas, Measuring the dispersion forces near the van der Waals–Casimir transition, Phys. Rev. Appl. **13**, 064057 (2020).

[16] R. Maboudian and R. T. Howe, Critical review: Adhesion in surface micromechanical structures, J. Vac. Sci. Technol. B **15**, 1 (1997).

[17] E. E. Parker, W. R. Ashurst, C. Carraro, and R. Maboudian, Adhesion characteristics of mems in microfluidic environments, J. Microelectromech. Syst. **14**, 947 (2005).

[18] J. A. Knapp and M. P. de Boer, Mechanics of microcantilever beams subject to combined electrostatic and adhesive forces, J. Microelectromech. Syst. **11**, 754 (2002).

[19] F. W. DelRio, M. P. de Boer, J. A. Knapp, E. D. Reedy, P. J. Clews, and M. L. Dunn, The role of van der Waals forces in adhesion of micromachined surfaces, Nat. Mater. **4**, 629 (2005).

[20] L. Vázquez, R. Salvarezza, P. Herrasti, P. Ocón, J. Vara, and A. Arvia, Scale-dependent roughening kinetics in vapor deposited gold, Surf. Sci. **345**, 17 (1996).

[21] Z. H. Liu, N. M. D. Brown, and A. McKinley, Evaluation of the growth behaviour of gold film surfaces evaporation-deposited on mica under different conditions, J. Phys.: Condens. Matter **9**, 59 (1997).

[22] A. I. Oliva, E. Anguiano, J. L. Sacedón, M. Aguilar, J. A. Méndez, and J. A. Aznárez, Extended statistical analysis of rough growth fronts in gold films prepared by thermal evaporation, Phys. Rev. B **60**, 2720 (1999).

[23] S. K. Sinha, E. B. Sirota, S. Garoff, and H. B. Stanley, X-ray and neutron scattering from rough surfaces, Phys. Rev. B **38**, 2297 (1988).

[24] R. Pynn, Neutron scattering by rough surfaces at grazing incidence, Phys. Rev. B **45**, 602 (1992).

[25] G. Palasantzas, Roughness spectrum and surface width of self-affine fractal surfaces via the k-correlation model, Phys. Rev. B **48**, 14472 (1993).

[26] P. J. van Zwol, V. B. Svetovoy, and G. Palasantzas, Distance upon contact: Determination from roughness profile, Phys. Rev. B **80**, 235401 (2009).

[27] D. F. Parsons, R. B. Walsh, and V. S. J. Craig, Surface forces: Surface roughness in theory and experiment, J. Chem. Phys. **140**, 164701 (2014).

[28] G. Palasantzas, D. Tsamouras, and J. De Hosson, Roughening aspects of room temperature vapor deposited oligomer thin films onto Si substrates, Surf. Sci. **507-510**, 357 (2002).

[29] See Supplemental Material at http://link.aps.org/supplemental/10.1103/PhysRevB.104.035415 for Table S1 and Figs. S1– S4.

[30] P. Meakin, The growth of rough surfaces and interfaces, Phys. Rep. **235**, 189 (1993).

[31] J. Krim and G. Palasantzas, Experimental observations of self-affine scaling and kinetic roughening at sub-micron lengthscales, Int. J. Mod. Phys. B **09**, 599 (1995).

[32] W. Broer, G. Palasantzas, J. Knoester, and V. B. Svetovoy, Roughness correction to the Casimir force beyond perturbation theory, Europhys. Lett. **95**, 30001 (2011).

[33] E. J. Gumbel, *Statistics of Extremes* (Dover, New York, 2004).

[34] M. Kardar, G. Parisi, and Y.-C. Zhang, Dynamic Scaling of Growing Interfaces, Phys. Rev. Lett. **56**, 889 (1986).

[35] T. Halpin-Healy and G. Palasantzas, Universal correlators and distributions as experimental signatures of (2+1)-dimensional Kardar-Parisi-Zhang growth, Europhys. Lett. **105**, 50001 (2014).